1 The global energy and water cycles

1.1 The global energy cycle

Richard D. Rosen

Introduction

Given the simple periodic forcing represented by solar radiation at the top of the atmosphere, it is rather remarkable to witness the extraordinary range in fluctuations present in the global climate system, fluctuations that span time and space on scales from millennia to seconds and from global to centimeters. This complexity arises not only from the dynamical nonlinearities inherent in the fluid components of the global system but also from the myriad interactions among those components, the land, and the biosphere. The existence of water in all three phases throughout the system adds further complexity, for water exerts a major influence on the transformation and exchange of the solar energy supplied to the system.

A framework for dealing with the complexities of the Earth system and predicting its response to perturbations comes to us from classical physics and involves tracing the flow of energy through the system, i.e. diagnosing the global energy cycle. Identifying the key processes involved in this cycle offers the promise of understanding how and why the system evolves. Because much of the energy flow in the Earth system is accomplished by atmospheric circulations, the study of the global energy cycle has been central to considerations of large-scale atmospheric behavior since at least the pioneering efforts of Starr (1951) and Lorenz (1955). The subject is well embedded in atmospheric survey texts (e.g. Wallace and Hobbs, 1977; Grotjahn, 1993) and is a focus of recent, extensive monographs (Peixoto and Oort, 1992; Wiin-Nielson and Chen, 1993). In light of this coverage elsewhere, no attempt at a comprehensive treatment of the global energy cycle is made here. Instead, the aim is to provide a brief overview of the subject while at the same time pointing out shortcomings that currently exist in our ability to observe and model the energy cycle.

Diagnoses of the energy cycle have yielded a general appreciation for the fundamental workings of the global atmosphere, but it is sobering to recognize how uncertain the estimates of many of the cycle's main components remain to this day. While such uncertainties may not have prevented a qualitative understanding of the mean state of the global system from being developed, they are a major hindrance to the sort of quantitative assessments needed today as attention turns to anomalies, both short-term and long, in the system. New observational techniques and a new willingness to address global-scale problems may help reduce these uncertainties, and so focusing attention on some of them here seems timely.

The global energy balance

The primary energy source and sink for the Earth are solar (shortwave) and terrestrial (longwave) radiation, respectively. Over the long term these two must balance, given that the planet is observed to be in thermal near-equilibrium. The manner in which the radiant energies are absorbed, emitted, scattered, or reflected is not constrained by this global equilibrium, however, and is vital in determining the response of the global system to the radiative forcing. It has become customary to display the various elements involved in the annual-mean global energy balance schematically; an example is given in Figure 1.1.

Of the 100 units of solar shortwave radiation incident at the top of the atmosphere (representing an irradiance of around 340 W m^{-2}), 31 units are reflected and scattered back to space by clouds, cloud-free air, and the surface, this proportion being the mean albedo of the planet. The remainder is absorbed partly in the atmosphere but, because of the atmosphere's large transparency to solar radiation, primarily by the surface, where it can be transformed into other forms of energy. A combination of longwave (i.e., infrared) radiation and sensible and latent heat fluxes are then returned from the surface to balance the absorbed solar radiation, as shown on the right-hand side of Figure 1.1. Of the longwave radiation emitted by the surface, most is absorbed in the atmosphere

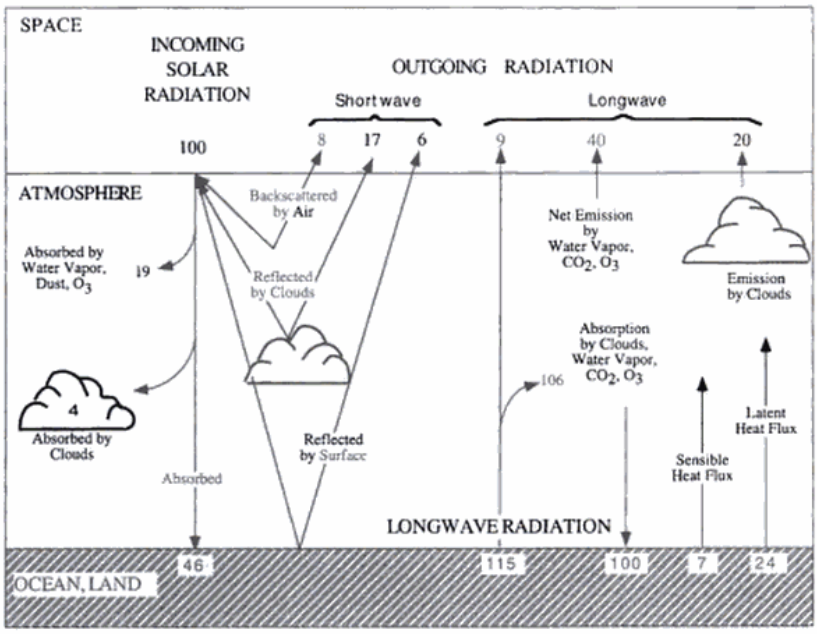

Figure 1.1. Schematic diagram of the annual-mean global energy balance. Units are percent of incoming solar radiation. The solar (shortwave) fluxes are shown on the left-hand side, and the terrestrial (longwave) fluxes are on the right-hand side. (From Mitchell, 1989.)

by clouds, water vapor, and other trace gases, only to be re-emitted out to space or back to the surface, this last process giving rise to the so-called greenhouse effect. Were it not for the additional surface warming caused by the re-radiation of infrared energy by the atmosphere, the mean surface temperature of the planet would be some 33 K colder.

Two points regarding Figure 1.1 are worth highlighting. The first concerns the ubiquitous influence of water in the global energy balance: water vapor and clouds interact with the radiation streaming through the system in critical ways. For example, more than half of the planetary albedo is due to clouds, and most of the infrared radiation emitted by the atmosphere is due to water vapor. Moreover, most of the net energy transferred from the surface to the atmosphere is in the form of latent heat associated with changes in phase of water substance. In combination with the smaller flux of sensible heat from the surface, the latent heat flux is responsible for maintaining a much cooler surface than would exist in the absence of these fluxes: if infrared radiation were the only mechanism to maintain the surface in thermal equilibrium, the surface would need to be more than 50 K hotter! From the viewpoint of the atmosphere, latent heat flux from the surface is the major process compensating for the roughly 2°C day^{-1} cooling that would otherwise result from the net loss of radiation by the atmosphere in Figure 1.1.

The second aspect of Figure 1.1 deserving comment regards the approximate nature of many of the values assigned to the various processes in the schematic. Although the values are based largely on observations, these may be incomplete in sampling or other respects and are often not direct. Hence, other versions of Figure 1.1 in the literature report different values, and although the discrepancies may appear slight, they can represent large amounts of energy, particularly when compared with the perturbations being studied in connection with global change. For example, according to the estimate reported in the figure, the amount of solar radiation absorbed by clouds and the rest of the atmospheric column is on the order of 80 W m^{-2}, but other estimates are as much as 15 W m^{-2} lower (Kiehl and Trenberth, 1997; Table 1). Some observations (Ramanathan *et al.*, 1995; Cess *et al.*, 1995, 1996) suggest, however, that the true value for solar absorption by the entire cloudy-sky column could be as much as 85 W m^{-2}, indicating that differences of 20 W m^{-2} or so exist in our current understanding of the shortwave radiation budget. Incorporating such differences in climate models can be expected to have a large impact on their climatologies, because of the attendant changes that would

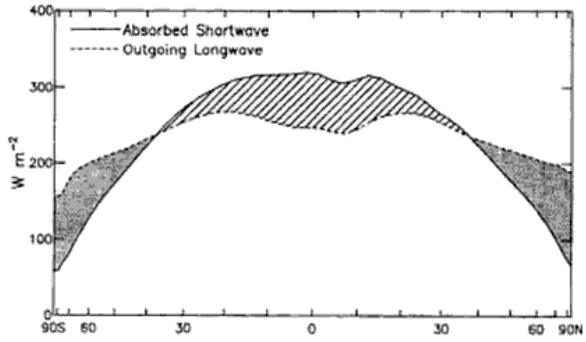

Figure 1.2. Zonally averaged annual mean top-of-the-atmosphere radiation from Earth Radiation Budget Experiment (ERBE) measurements for 1988 as a function of latitude. Shown are the absorbed shortwave (solar) radiation (solid line) and outgoing longwave radiation (dashed line), with their difference, representing the net radiational forcing, highlighted. (From Trenberth and Solomon, 1994.)

occur in other parts of the energy budget, such as the latent heat flux and, therefore, in the models' hydrologic cycles (see, for example, Kiehl *et al.*, 1995). The possibility of enhanced shortwave absorption by clouds is a controversial issue, however (Wiscombe, 1995; Arking *et al.*, 1996; Crisp, 1997), and measurement campaigns are under way to help resolve it. Clearly, effort is needed in placing all the values shown in Figure 1.1 on as firm a foundation as possible.

Flow of energy in the climate system: the role of atmospheric and oceanic circulations

The schematic of Figure 1.1 provides a globally averaged view of the Earth's energy budget, but important consequences for the planet's climate, including the general circulation of the atmosphere, arise from latitudinal differences in this budget. Figure 1.2 displays meridional profiles of the solar radiation absorbed by the Earth–atmosphere–ocean system (i.e., the incoming solar radiation minus that reflected back to space) and of the longwave radiation emitted by the planet out to space. In principle, the integral under each curve should be the same if thermal equilibrium exists, although Trenberth and Solomon (1994) note that the satellite data used to create Figure 1.2 contain a small imbalance of around 4 W m^{-2}. The most striking, and critical, aspect of the figure, though, relates to the very different shapes of the two profiles. Because of the Earth's shape and orbital characteristics, the amount of solar energy reaching the top of the atmosphere varies sharply with latitude: values near the Equator are more than a factor of two larger than those near the poles in the annual mean. This contrast is even more pronounced for the absorbed solar radiation plotted in the figure, because of the larger albedo in (snow- and ice-covered) polar regions than in the tropics. Outgoing terrestrial radiation, on the other hand, is solely a function of the temperature at which it is emitted and is therefore considerably less dependent on latitude.

The resulting difference between the two curves, i.e., the net radiation, demonstrates that most of the planet is not in local radiative equilibrium. At low latitudes, the amount of radiation absorbed exceeds that emitted; the reverse is true at high latitudes. To achieve a balance in each region, the atmosphere and ocean transport energy from the tropics towards the poles. Within the atmosphere, the mode of transport is governed by the nature of the forces acting to accelerate air parcels, including the pressure gradient force that arises from the meridional contrast in heating. A thermally direct circulation, the 'Hadley cell', develops in the tropics in response to the heating contrast, but the temperature gradient across mid-latitudes is of such a magnitude relative to the effects of the Earth's rotation that large-scale waves become a more efficient means of transporting heat. This combination of a Hadley regime in the tropics and an eddy regime in the extratropics constitutes the general circulation of the atmosphere.

The energy transported by the planet's fluid envelope can assume a number of forms. The main forms in the atmosphere are internal energy I, potential energy Φ, kinetic energy K, and latent energy associated with (liquid-vapor) phase transitions of water L. Expressions for these energy forms per unit mass are:

$$I = c_v T \tag{1.1.1}$$

$$\Phi = gz \tag{1.1.2}$$

$$\mathrm{K} = \tfrac{1}{2}(u^2 + v^2 + w^2) \approx \tfrac{1}{2}\boldsymbol{v}\cdot\boldsymbol{v} \tag{1.1.3}$$

$$\mathrm{L} = Lq \tag{1.1.4}$$

where c_v is specific heat at constant volume, T temperature, g acceleration due to gravity, z geopotential height above the surface, u zonal wind, v meridional wind, w vertical velocity, $\boldsymbol{v}$ horizontal wind vector, L latent heat of evaporation, and q specific humidity. It can be shown that because the atmosphere is very nearly in hydrostatic equilibrium, the internal and potential energies in a vertical column are proportional to each other, and so it is customary to consider instead their sum, which for a column is given by

$$\int_0^\infty \rho c_p T \mathrm{d}z$$

where ρ is density and c_p is specific heat at constant pressure. This integral represents the enthalpy in an atmospheric col-

umn, but it is also sometimes referred to as the total potential energy.

An equation governing the balance of energy in the atmosphere can be derived in isobaric coordinates from the horizontal equations of motion, the thermodynamic equation, the mass continuity equation, and the moisture equation. The resulting energy balance equation may be written in differential form as

$$\frac{\partial}{\partial t}(c_p T + Lq + K) + \nabla\cdot(s + Lq + K)\,\boldsymbol{v} + \frac{\partial}{\partial p}(s + Lq + K)\omega = Q \qquad (1.1.5)$$

where p is pressure, ω vertical velocity in isobaric coordinates, $s = c_p T + \Phi$ dry static energy, and Q diabatic heating involving transfers of heat due to radiative, sensible, latent, and/or frictional processes. The dry static energy s incorporates mechanical work done by the pressure force (which appears as a flux of potential energy in the equation) and, when combined with the latent energy, forms the moist static energy ($h = s + Lq$) of the atmosphere.

Because the kinetic energy is several orders of magnitude smaller than the total potential energy of the atmosphere, its contribution in the above equation can be neglected. Upon integrating the equation vertically through the depth of the atmosphere, we then obtain

$$\frac{1}{g}\int\frac{\partial}{\partial t}(c_p T + Lq)\,\mathrm{d}p + \frac{1}{g}\int\nabla\cdot h\boldsymbol{v}\,\mathrm{d}p = F_T - F_B \qquad (1.1.6)$$

where F_T and F_B are the net downward fluxes of energy at the top and bottom of the atmosphere, respectively. Note that F_T consists simply of the net radiative flux at the top of the atmosphere, but F_B will include radiative, sensible, and latent heat fluxes at the surface. The equation above states that the net vertical flux of energy into an atmospheric column ($F_T - F_B$) can act either to change the total atmospheric energy of the column (the first term on the left-hand side) or to induce horizontal transports of moist static energy out of the column. Because the meridional contrast in net radiative heating (Figure 1.2) dominates the shaping of $F_T - F_B$, the energy balance equation is often further integrated over a polar cap volume whose lateral boundary is a latitudinal wall, so that meridional transports of energy become an explicit focus:

$$\frac{\partial}{\partial t}\int(c_p T + Lq)\,\mathrm{d}m = \frac{1}{g}\int_{\text{wall}}\int h v\,\mathrm{d}x\mathrm{d}p + (F_T - F_B) \qquad (1.1.7)$$

where $\mathrm{d}m$ is an element of atmospheric mass and $\mathrm{d}x$ is unit distance in the zonal direction. On an annual-mean basis, changes in energy stored within an atmospheric volume are small, so the left-hand side of the equation becomes zero, and a balance is achieved between fluxes of moist static energy across the latitudinal wall of a polar cap volume and the net flux of energy across the volume's upper and lower boundaries.

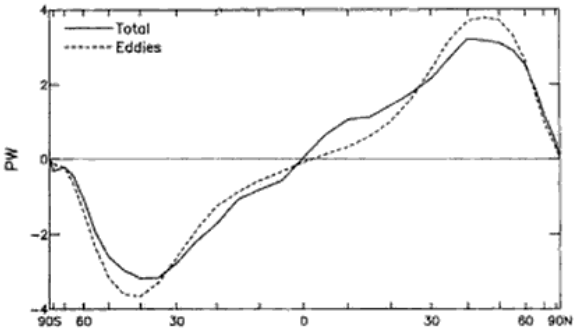

Figure 1.3. Meridional profiles of the annual-mean, total northward transport of moist static energy by the atmosphere (solid line) and of the component due to the sum of transient and stationary eddies (dashed line), derived from analyses of radiosonde observations by Oort and Peixoto (1983) for May 1963 to April 1973.

The annual-mean meridional flux of moist static energy in the atmosphere can be computed from upper-air analyses of wind, temperature, and humidity fields based on observations taken at the global network of radiosonde stations. An example is shown in Figure 1.3 from the analysis of Oort and Peixoto (1983) for the 10-year period from May 1963 through April 1973. In addition to the total flux, the figure also includes the contribution made by eddies to the total. Note that the total flux peaks in mid-latitudes where the region of excess net radiation in the tropics is separated from the region of net radiation deficit in higher latitudes (cf. Figure 1.2). Eddies are clearly the dominant mechanism in the atmosphere for accomplishing the required annual-mean poleward transport of energy. At the latitudes of peak flux, almost half of the transport is in the form of latent energy (Figure 1.4), once again attesting to the importance of water and water vapor to the global energy cycle.

The estimates of meridional energy fluxes shown in Figures 1.3 and 1.4 are subject to numerous uncertainties related to the imperfect sampling of the atmosphere by the radiosonde network. Stations are especially scarce over the oceans and tropical continents, adversely affecting the calculation of net meridional fluxes, particularly in low and southern latitudes. Approaches using the global analyses of operational weather forecast centers, such as the US National Centers for Environmental Prediction or the European Centre for Medium-range Weather Forecasts (ECMWF), have become popular alternatives, because such analyses utilize observations not only

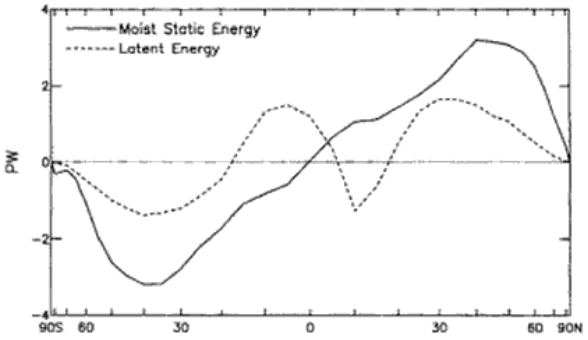

Figure 1.4. Meridional profiles of the annual-mean, total northward transport of moist static energy by the atmosphere (solid line) from Figure 1.3 and of the part due to the total transport of water vapor and its latent energy (dashed line), derived from analyses of radiosonde observations by Oort and Peixoto (1983) for May 1963 to April 1973.

from radiosondes but also from other available platforms, and blend all the observations together in a dynamically consistent manner with a 'first guess' produced by a numerical weather prediction (NWP) model. The output from these operational analyses is available in a convenient, gridded format, allowing calculations to be made readily. Differences in the net meridional flux of moist static energy between radiosonde-based and operational NWP-based analyses can amount to 1 PW (1 PW = 10^{15} W) or more (Michaud and Derome, 1991). Whereas it is tempting to assign most of this discrepancy to errors in the radiosonde-based values, substantial shortcomings also exist in the operational analyses (Trenberth and Solomon, 1994). These include the strong dependence of the analyses upon the verisimilitude of the NWP model in data-sparse regions and the assumptions made in blending values from the model with observations.

Determining the meridional energy flux for the oceans from direct observations is even more problematic than for the atmosphere, because of the general scarcity of ocean measurements. A few direct oceanic calculations do exist, however, such as the value of 2.0 PW across 24°N reported by Bryden (1993). A more common approach has been to infer the ocean transport indirectly from top-of-the-atmosphere radiation budget considerations. This approach takes advantage of the atmospheric energy balance equation written earlier, namely,

$$\frac{1}{g}\int \nabla\cdot h\,\boldsymbol{v}\,\mathrm{d}p = F_{\mathrm{T}} - F_{\mathrm{B}} \tag{1.1.8}$$

(where the storage term has been disregarded) and the direct measurements of the atmospheric flux to evaluate the left-hand side of this equation. Satellite measurements provide estimates of F_{T}, so that F_{B} can then be obtained as a residual. Because one may assume that over an annual period the land is in thermal equilibrium and there are no horizontal transports of heat within the land, F_{B} equals zero there. Hence, the value of F_{B} obtained as a residual must apply entirely over the oceans. With this boundary condition and the assumption that thermal equilibrium is maintained within the oceans, the required ocean transport of heat may be inferred, usually on the basis of zonal-mean values.

The indirect estimate of ocean heat transport incorporates uncertainties in the calculation of atmospheric heat transports mentioned above, and it is also sensitive to small biases in the satellite measurements of solar and terrestrial radiation at the top of the atmosphere. Both sources of error can together easily account for a one petawatt or so difference between most indirect and direct estimates of ocean heat transport. Note that because $F_{\mathrm{B}} = 0$ over land, the last equation reduces to

$$\frac{1}{g}\int \nabla\cdot h\,\boldsymbol{v}\,\mathrm{d}p = F_{\mathrm{T}} \text{ (over land)} \tag{1.1.9}$$

so that a balance should exist between the atmospheric energy flux divergence and F_{T} over land. Trenberth and Solomon (1994) point out, however, that this balance is, in fact, not generally satisfied in the atmospheric data sets normally used to infer the ocean heat flux, and so zonal-mean calculations of this flux are flawed. Instead, Trenberth and Solomon (1994) solve a Poisson equation for the *local* divergence of the ocean heat flux that is forced by F_{B} and is subject to the boundary condition of no flux through the continental boundaries. Although adjustments to the results are still necessary because of errors in the residual F_{B} field, this method leads eventually to zonal-mean meridional ocean heat fluxes that agree better with the direct ocean estimates. Although it is possible that the problem of the 'missing petawatt' can thus be resolved by recognizing the shortcomings present in the atmospheric measurements and analyses, it is important to remember that considerable uncertainties still exist in both the indirect and direct ocean heat transport estimates (Gleckler, 1993; Trenberth and Solomon, 1994).

In summary, the error bars on global energy transports by the atmosphere and ocean remain large, and concerted efforts will be required to reduce them to the point where useful information about the variability of the energy budget on climate-related time scales can be obtained. Nevertheless, the results of Trenberth and Solomon (1994) for an annual mean are illuminating (Figure 1.5). It is clear that both atmosphere and oceans play important roles in effecting the pole-

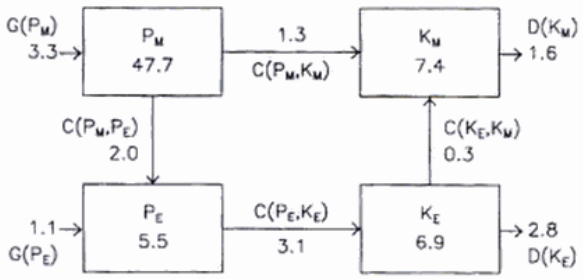

Figure 1.6. Global annual-mean atmospheric energy cycle for the FGGE year (December 1978 to November 1979), from Kung (1986). As defined in the text, available potential (P) and kinetic (K) energies are separated into zonal-mean and eddy components, indicated by the subscripts M and E respectively; units of energy are 10^5 Jm^{-2}. (Note that it is customary in these diagrams to report the values of the various energies themselves rather than their mean time rates of change, as is strictly called for by the balance equations. The latter are typically very small, however, and so can be safely neglected.) Conversions from one energy form to another (symbolized by the letter C), generations of available potential energy (symbolized by G), and frictional dissipations of kinetic energy (symbolized by D) are all reported in units of W m^{-2}.

from different physical processes to be separated for further study. An alternative method which permits such a separation is to utilize the heating fields generated by the 'physics package' of the NWP model used in assimilating the wind and temperature observations. Results from this alternative approach, however, tend to be sensitive to the parameterization schemes used in the physics package and to suffer from sampling and other difficulties as well (Fortelius, 1995). Hence, quantitative assessments of the role of, say, latent heating in generating zonal-mean available potential energy remain highly uncertain, although it does appear (Salstein and Sud, 1994) that this process is the major contributor to the positive, annual-mean value found for $G(P_M)$. This result appears to stand in marked contrast to the role of latent heating within the tropics, where Emanuel *et al.* (1994) suggest that convection acts to damp larger-scale circulations, implying that $G(P_E)$ due to latent heating within the tropics is negative.

To close this section on the atmospheric energy cycle, it is appropriate to raise the issue of how efficient a heat engine the atmosphere is. Lorenz (1967) remarked that 'the determination and explanation of the efficiency [of the atmospheric heat engine] constitute the fundamental observational and theoretical problems of atmospheric energetics', and this perspective remains valid today. The efficiency η of the atmosphere is constrained to be relatively small by the pole-to-Equator temperature difference: for the ideal case of a Carnot engine,

$$\eta = (T_W - T_C)/T_W$$

where T_W is the temperature of the warm source and T_C that of the cold sink, which would make η less than about 10% for the atmosphere. Other definitions of η are appropriate, however; for example, one may regard η to be the ratio of the rate at which kinetic energy is produced by the atmosphere to the rate at which solar energy reaches the top of the atmosphere, in which case η is on the order of only 1%.

Regardless of precisely how the efficiency is defined, it is intriguing to inquire as to whether the atmosphere is operating as efficiently as it can under present conditions. Phrased differently, one may wonder what factors limit the strength of the winds in the current climate and whether such factors may be altered in a different climate scenario. These questions seem not to be addressed often in the literature, but early works by Schulman (1977) and by Lin (1982) do suggest that the general circulation is operating near maximum efficiency, or at least within a factor of about two of doing so. This conclusion remains tentative, however, and deserves further investigation.

Final remarks

As noted at the outset, the application of energy principles to the study of the global climate system helps place this study on firm physical grounds. It also illuminates, in broad terms, the workings of the general circulation of the atmosphere. Our ability to measure the flow of energy through the system, however, has not advanced to the stage where we can reliably quantify behavior on a variety of time scales. Significant seasonal variations in the energy cycle exist, of course, and are generally understood, at least qualitatively. Space limitations here do not permit a discussion of these seasonal aspects, but such a discussion would emphasize the moderating influence of the oceans on climate. Because of their large heat capacity, the oceans can release to the atmosphere substantial amounts of heat during winter that they accumulated during summer. In the Northern Hemisphere especially, the contrast between the heat capacities of ocean and land imparts a strong seasonal, and non-zonal, signature to the long-term mean circulation. Variations in ocean heat storage on other time scales are also critical in explaining the existence of such notable interannual fluctuations in atmospheric circulation and climate as those associated with the tropical El Niño/Southern Oscillation phenomenon (Philander, 1990).

Our understanding of the energetics of the climate system

and its variability is limited by the fact that transfers of heat within the system associated with diabatic processes remain notoriously difficult to observe and quantify. Uncertainties in the energy generation terms due to these processes can be comparable to the size of the energy conversions which drive the general circulation in Figure 1.6. Techniques for estimating diabatic processes using data assimilation models are emerging, but for the present these estimates are also highly uncertain. The challenge of accurately quantifying anomalies or trends in the global energy cycle is daunting, but with concerted effort, there is reason to believe that it can be met.

1.2 The global water cycle

Taikan Oki

The total volume of water on the Earth is estimated as approximately 1.4×10^{18} m^3, and it corresponds to a mass of 1.4×10^{21} kg. Compared with the total mass of the Earth (5.974×10^{24} kg), the mass of water constitutes only 0.02% of the planet, but it is critical for the survival of life on the Earth. There are various forms of water on the Earth's surface. Approximately 70% of its surface is covered with salty water, the oceans. Some of the remaining area (continents) are covered by fresh water (lakes and rivers), solid water (ice and snow), and vegetation (which implies the existence of water). Even though the water content of the atmosphere is comparatively small (approximately 0.3% by mass and 0.5% by volume of the atmosphere), approximately 60% of the Earth is always covered by cloud (Rossow *et al.*, 1993). The Earth is the planet whose surface is dominated by the various phases of water.

Before addressing the water cycle, it is necessary to consider the budget of total water on the Earth. Hot springs and water vapor ejected from volcanoes seem to be the major sources, but most of this is recycled water. The generation of juvenile water from the interior of the solid Earth to its surface has been roughly estimated as 1.0×10^{11} kg year^{-1} (Kuenen, 1963), and is negligible compared with the total mass of water at the Earth's surface. A certain amount of water vapor may be destroyed in the upper atmosphere through photodissociation by solar radiation, but it is also relatively negligible. The H_2O molecule is too heavy to escape from the Earth's gravity. The other source and sink terms are the generation and decomposition of water by respiration and photosynthesis, but they are expected to be balanced. Water is also released by the burning of fossil fuels

$$(CH_2O)_n + nO_2 \rightarrow nCO_2 + nH_2O$$

The same number of water molecules as carbon dioxide molecules is made by this process. With the carbon emissions from fossil fuels at 5×10^{12} kg year^{-1} (Marland and Rotty, 1984), the emission of water should be 7.5×10^{12} kg year^{-1}. This, too, is negligible compared with the total water on the Earth's surface. Altogether, the total amount of water on the Earth can be regarded as constant on the time scale of up to thousands of years that we are concerned with here.

It is also important to consider how much water is associated with each subsystem (reserve) of the water cycle; see Table 1.1 (simplified from a table in Korzun, 1978). The proportion in the ocean is large (96.5%). Other major reserves are solid water on the continent (glaciers and permanent snow cover) and ground water. Ground water in Table 1.1 includes both gravitational and capillary water. Gravitational water is water in the unsaturated zone (vadose zone) which moves under the influence of gravity. Capillary water is water in the soil above the water table by capillary action, a phenomenon associated with the surface tension of water in soils acting as porous media. Ground water in Antarctica (roughly estimated as 2×10^6 km^3) is excluded from Table 1.1. The amount of water stored transiently in a soil layer, in the atmosphere, and in river channels is relatively minute, and the time spent through these subsystems is short, but, of course, they play dominant roles in the global hydrologic cycle.

The objective of this section is to illustrate the global water cycle as quantitatively as possible by means of the latest global data sets. Some of the values and distributions presented here may be different from those in other chapters, emphasizing the uncertainty in our current knowledge of the global water cycle. The precise numbers in the figures and tables will change in the future through the development and use of more dense and comprehensive observing systems, but the framework of the global water cycle that is presented is believed to be valid.

Nature of the water cycles in the climate system

The global hydrologic cycle is one of the key elements in the global environment. Any change in precipitation, evapotranspiration, or runoff may have serious effects for societal activities, and quantitative estimation of the current and future hydrologic cycle is crucial for planning purposes. Climate change, caused either by natural variability of the climate system or by the increases of carbon dioxide and other greenhouse gases by anthropogenic activities, may have important impacts on the water cycles.

The water cycle plays many important roles in the climate system via its various subsystems. Figure 1.7 schematically illustrates the subsystems of the water cycle. Values are taken from Table 1.1 and also calculated from the precipitation estimates by Xie and Arkin (1996). Precipitable water, water vapor transport, and its convergence are estimated using ECMWF (European Centre for Medium-range Weather Forecasts) objective analyses, obtained as 4-year means from 1989 to 1992. The roles of these subsystems in the climate system are now briefly introduced.

Table 1.1. *World water reserves.*

Form of water	Covering area (km^2)	Total volume (km^3)	Mean depth (m)	Share (%)
World ocean	361 300 000	1 338 000 000	3 700	96.539
Glaciers and permanent snow cover	16 227 500	24 064 100	1 463	1.736
Ground water	134 800 000	23 400 000	174	1.688
Ground ice in zones of permafrost strata	21 000 000	300 000	14	0.0216
Water in lakes	2 058 700	176 400	85.7	0.0127
Soil moisture	82 000 000	16 500	0.2	0.0012
Atmospheric water	510 000 000	12 900	0.025	0.0009
Marsh water	2 682 600	11 470	4.28	0.0008
Water in rivers	148 800 000	2 120	0.014	0.0002
Biological water	510 000 000	1 120	0.002	0.0001
Total water reserves	510 000 000	1 385 984 610	2 718	100.00

Note: Simplified from Table 9 of Korzun (1978).

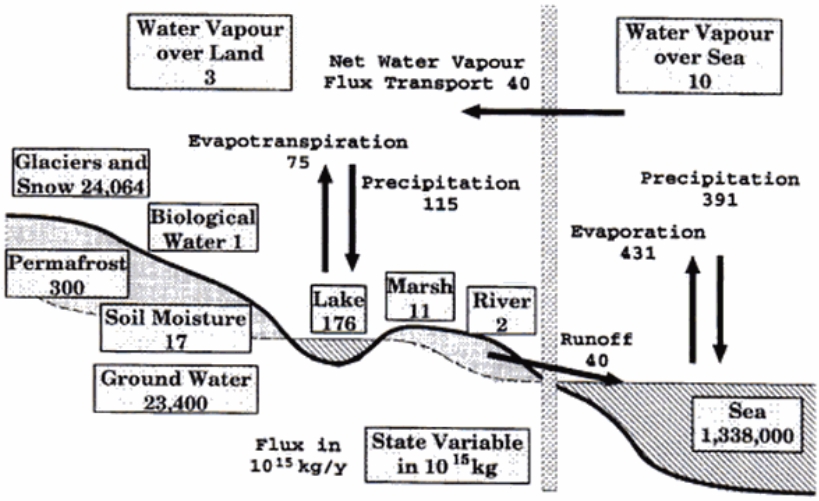

Figure 1.7. Schematic illustration of the water cycle on the Earth. Values are taken from Table 1.1 and calculated from atmospheric water vapor data by ECMWF and precipitation by Xie and Arkin (1996) for 1989–92.

The atmosphere carries *water vapor*, which influences the heat budget as latent heat. Condensation of water releases latent heat, heats up the atmosphere, and affects the atmospheric general circulation. Water vapor is also the major absorber in the atmosphere of both shortwave and longwave radiation.

Liquid water in the atmosphere is another result of condensation. *Clouds* significantly change the radiation in the atmosphere and at the Earth's surface. *Precipitation* drives the hydrologic cycle on the land surface and changes surface salinity over the ocean.

Snow has special characteristics compared with rainfall. Snow may be accumulated, the albedo of snow is quite high (as high as clouds), and the surface temperature will not rise above 0°C until the completion of snow melt. Consequently the existence of snow changes the surface

energy budget enormously. A snow surface typically reduces the aerodynamic roughness, so that it may also have a dynamical effect on the atmospheric circulation.

Evaporation is the return flow of water from the surface to the atmosphere and gives the latent heat flux from the surface. The amount of evaporation is determined by both atmospheric and hydrologic conditions. From the atmospheric point of view, the fraction of incoming solar energy to the surface leading to latent and sensible heat flux is important. Wetness at the surface influences this fraction because the ratio of actual evapotranspiration to the potential evaporation is reduced due to drying stress. The stress is sometimes formulated as a resistance.

Transpiration is the evaporation of water through stomata of leaves. It has two special characteristics different from evaporation from soil surfaces. One is that the resistance of stomata is related not only to the dryness of soil moisture but also to the physiological conditions of the vegetation through the opening and the closing of stomata. Another is that roots can transfer water from deeper soil layers than in the case of evaporation from bare soil. Vegetation also modifies the surface energy and water balance by altering the surface albedo and by intercepting precipitation and evaporating this rain water.

Soil moisture influences the energy balance at the land surface as a lack of available water suppresses evapotranspiration and as it changes surface albedo. Soil moisture also alters the fraction of precipitation partitioned into direct runoff and percolation. The water accounted for in runoff cannot be evaporated from the same place, but the water infiltrated into soil layers may be evaporated again.

Ground water is the subsurface water occupying the saturated zone. It contributes to runoff in its low-flow regime, between floods. Deep ground water may also reflect the long-term climatological situation.

Runoff returns water to the ocean which may have been transported in vapor phase by atmospheric advection far inland. The amount of water mass carried by rivers is smaller than that carried by the atmosphere and oceans, but yet it is not negligible. The runoff into oceans is also important for the freshwater balance and the salinity of the oceans.

Ocean is a giant subsystem of the global water cycle. Even though classical hydrology has traditionally excluded ocean processes, the global hydrologic cycle is never closed without including them. The ocean circulation carries huge amounts of energy and water. The surface ocean currents are driven by surface wind stress, and the atmosphere itself is sensitive to the sea surface temperature. Temperature and salinity determine the density of ocean water, and both factors contribute to the overturning and the deep ocean general circulation.

The global water cycle unifies the subsystems consisting of the state variables (precipitable water, soil moisture, etc.) and the fluxes (precipitation, evaporation, etc.).

Water balance requirements

The conservation law of water mass in any arbitrary control volume implies a water balance. In this section, the water balance of land surface, atmosphere, and their combination are presented. Some applications are also introduced.

Water balance at land surface

In the field of hydrology, river basins have commonly been selected for study, and water balance has been estimated using ground observations, such as precipitation, runoff, and storage in lakes and/or ground water.

The water balance at land surface is described as

$$\frac{\partial S}{\partial t} = -\nabla_H \cdot \vec{R}_o - \nabla_H \cdot \vec{R}_u - (E - P) \tag{1.2.1}$$

where S represents the water storage within the area, $\vec{R}_o$ is surface runoff, $\vec{R}_u$ is the ground water movement, E is evapotranspiration, and P is precipitation. The term $\nabla_H \cdot$ represents the horizontal divergence. S includes snow accumulation in addition to soil moisture, ground water, and surface water storage including retention water. These terms are shown in Figure 1.8(*a*). If the area of water balance is set within an arbitrary boundary, $\nabla_H \cdot \vec{R}_o$ represents the net outflow of water from the region of consideration (i.e., the outflow minus total inflow from surrounding areas). Generally it is not easy to estimate ground water movement $\vec{R}_u$, and the net flux per unit area within a large area is expected to be comparatively small. In this section, all ground water movement is considered to be that observed at the gauging point of a river ($\nabla_H \cdot \vec{R}_u = 0$), and equation (1.2.1) becomes:

$$\frac{\partial S}{\partial t} = -\nabla_H \cdot \vec{R}_o - (E - P) \tag{1.2.2}$$

Water balance in the atmosphere

It is known in the field of climatology that atmospheric water vapor flux convergence gives water balance information that can complement the traditional hydrologic elements such as

Table 1.2. *Global water balance ($-\nabla_H \cdot \vec{Q} = P - E = R$) estimates (mm year^{-1}) over oceans.*

All oceans	Arctic	Indian	Pacific	Atlantic	
−111	50	−250	91	−384	Baumgartner and Reichel (1975)
−132	263	−97	−56	−333	Korzun (1974)
−18	(in Atlantic)	−53	20	−136	Bryan and Oort (1984)
−66	163	−113	12	−190	Masuda (1988), ECMWF–FGGE
−114	175	−147	14	−345	Masuda 1988, GFDL–FGGE
−78	185	−126	6.3	−236	Oki *et al.* (1995*b*), ECMWF 1985–88
−115	208	−198	−6.7	−299	Oki *et al.* (1995*c*), ECMWF 1989–92

Table 1.3. *Global water balance ($-\nabla_H \cdot \vec{Q} = P - E = R$) estimates (mm year^{-1}) over continents.*

All	Asia	Eur.	Afr.	N.A.	S.A.	Au.	Ant.	
256	260	255	113	223	611	267	143	Baumgartner and Reichel (1975)
269	281	273	140	258	578	222	157	Lvovitch (1973)
303	300	273	153	315	678	278	164	Korzun (1978)
42	32	−181	7	162	333	−400	43	Bryan and Oort (1984)
152	94	164	63	227	422	56	100	Masuda (1988), ECMWF–FGGE
260	100	91	333	223	850	211	107	Masuda (1988), GFDL–FGGE
165	235	136	−100	263	415	54	112	Oki *et al.* (1995*b*), ECMWF 1985–88
244	244	197	4	318	773	24	130	Oki *et al.* (1995*c*), ECMWF 1989–92

Note: Mean over continents, Asia, Europe, Africa, North America (N.A.), South America (S.A.), Australia, and Antarctica.

trative of what can be obtained now and as providing an indication of future prospects.

Atmospheric water balance estimation

Twice-daily data sets from ECMWF, analyzed objectively by the 4-dimensional assimilation technique, are used in this subsection. Precipitable water W and water vapor flux convergence $-\nabla_H \cdot \vec{Q}$ are calculated by equations (1.2.4), (1.2.5), and (1.2.7) using algorithms described in Oki *et al.* (1995*b*). Monthly and annual mean values are integrated from the twice-daily estimates of W, $\vec{Q}$, and $-\nabla_H \cdot \vec{Q}$. The sampling effect on such estimates is discussed by Phillips *et al.* (1992). One problem is the diurnal variation which, especially in tropical areas, is very large (e.g., Oki and Musiake, 1994). Trenberth and Guillemot (1995) compared estimates of monthly means based on twice daily data and four times daily data. They found that the differences of W were regional and went up to 0.5 mm throughout the tropics. Such errors can be neglected. The differences of $-\nabla_H \cdot \vec{Q}$ were 10–20 mm month^{-1} over a limited tropical region, and rms differences averaged around latitude circles were 30–60 mm month^{-1} regionally. Thus the diurnal cycle is significant for divergence estimates.

The model used in the ECMWF analyses has changed many times; major changes occurred on 1 May 1985 and 2 May 1989. Therefore 4-year means for the periods 1985 to 1988 and 1989 to 1992 were examined for their accuracy. Specific aspects that were checked were:

- the negative areas of 4-year mean vapor flux convergence ($-\nabla_H \cdot \vec{Q} < 0$) over land (refer ahead to Figure 1.10*a*),
- the water balance ($-\nabla_H \cdot \vec{Q}$) over oceans and continents (see Tables 1.2 and 1.3), and
- the degree of quantitative correspondence between $-\nabla_H \cdot \vec{Q}$ and river runoff (refer ahead to Figure 1.15).

A region with negative annual water vapor flux convergence is where the annual evaporation exceeds the annual precipitation (see equation (1.2.10)). Such a situation may occur over land at some part of an inland river basin or at the downstream end of a large river; however, most of these estimates are probably erroneous. In addition, one has to be careful in that $P - E$ estimated by the model will not generally agree with $-\nabla_H \cdot \vec{Q}$ in the 4-dimensional data assimilation

cycle, because such a model has its own bias, and an artificial supply or extraction of water vapor is applied during the assimilation cycle. It is believed that improvements in data and in the treatment of the surface may eliminate the negative annual convergence regions over land on the global scale.

Annual water vapor flux convergence estimates are compared with earlier estimates in Table 1.2 and Table 1.3 based on equation (1.2.10). Baumgartner and Reichel (1975), Lvovitch (1973), and Korzun (1978) estimated runoff by hydrological methods using surface observations. Others listed in these tables used the atmospheric water balance method. Note in the case of Bryan and Oort (1984), the Middle East is included in Europe, not in Asia, and the Arctic Ocean is included in the Atlantic Ocean. The signs of $-\nabla_H \cdot \vec{Q}$ in Table 1.2 are mostly the same among the estimates, but the absolute values vary. In the Pacific Ocean, the precipitation and evaporation approximately balance each other. Evaporation exceeds precipitation in the Atlantic and Indian Oceans, and vice versa in the Arctic Ocean. In Table 1.3, results from the hydrologic method produce broadly similar estimates compared with those by the atmospheric water balance method, although estimates by atmospheric data tend to be generally smaller than the hydrologic estimates. The annual river runoff averaged over the area of a continent is approximately 200–300 mm year^{-1} except for South America, where the estimated annual runoff is 400–800 mm year^{-1}. Continents with high aridity (Africa) and with very cold regions (Antarctica) have small runoff.

The global mean continental discharge (see the first column in Table 1.3) of the 1989–92 mean, 244 mm year^{-1}, is closer to the hydrologic estimates than that of the 1985–88 mean (165 mm year^{-1}). From these comparisons, the 4-year mean of 1989–92 is used here as a good representation of our current knowledge of the global aspects of water and its transport in the atmosphere.

Global aspects of atmospheric water vapor storage, transport, and divergence

The annual mean over the global ocean for precipitable water W is estimated as 28.4 mm using ECMWF data from 1989 to 1992. This value is close to the 28.9 mm estimated by Trenberth and Guillemot (1994) using 4-year data of ECMWF from July 1987 to June 1991, but they found this to be larger than that of Special Sensor Microwave/Imager (SSM/I) satellite estimates of 26.8 mm for the same period for the corresponding global ocean. The SSM/I estimates are regarded as more credible, in which case the ECMWF estimates presented below may be overestimated by 10%. The annual mean W over the globe before any such correction is 26.1 mm, and 21.1 mm over land.

Zonal means (i.e., averages in an east–west direction) of precipitable water, averaged over (a) land and sea, (b) land only, and (c) sea only are shown in Figure 1.9. Annual, December–January–February (DJF), and June–July–August (JJA) means are shown in each figure, and the length of the horizontal axis is proportional to the area at each latitude ($\cos(\phi)$). The fraction of land at each latitude is shown by bars in Figure 1.9(*b*). Zonal mean values are of interest because the atmosphere is comparatively more uniform in the east–west direction than in the north–south direction. A particular point of interest is to see how the distribution of zonal means departs from north–south symmetry, because the radiative forcing is nearly equal for both hemispheres in the annual mean, even though the solar irradiance is larger by a few percent in January. One of the major differences between the characteristics of the two hemispheres is in the fraction of sea and land. More than 40% is covered by land in the northern hemisphere, but only 20% in the southern hemisphere.

It is worth considering the water cycle over land and sea separately. Sea water has large heat capacity and large volume. Water over oceans can evaporate as required and the changes of surface temperature are relatively small. However, evapotranspiration over land is suppressed with a deficit of water storage over land, and the surface temperature is determined as a result from land–atmosphere coupling of energy and water. Accordingly, the Bowen ratio (the ratio of sensible heat flux to latent heat flux) may differ over land and sea.

The peak of zonal mean W is situated at 10°N for the overall mean (Figure 1.9*a*) and for the mean over sea (Figure 1.9*c*). The zonal mean W over land (Figure 1.9*b*) is nearly symmetrical about the Equator for the annual mean, and the DJF mean is close to the mirror image of the JJA mean between 40°S and 40°N. The water vapor content in the atmosphere is highly sensitive to the temperature through the saturation vapor pressure (e_s), and the temperature (which determines the e_s via a monotonic exponentially increasing function) decreases toward the upper atmosphere. As a result, more than 50% of the water vapor is concentrated below the 850 hPa surface, and more than 90% is confined to the layer below 500 hPa (Peixoto and Oort, 1992*b*). Therefore we can consider that the W-field corresponds closely to the surface temperature over the ocean (Stephens, 1990). The fact that the difference in mean W between DJF and JJA is larger over land than sea is due to the large annual difference of surface temperature over continents and the relatively small change of sea surface temperature.

Global distributions of vertically integrated water vapor flux convergences $-\nabla_H \cdot \vec{Q}$ are shown in Figure 1.10. Tropical

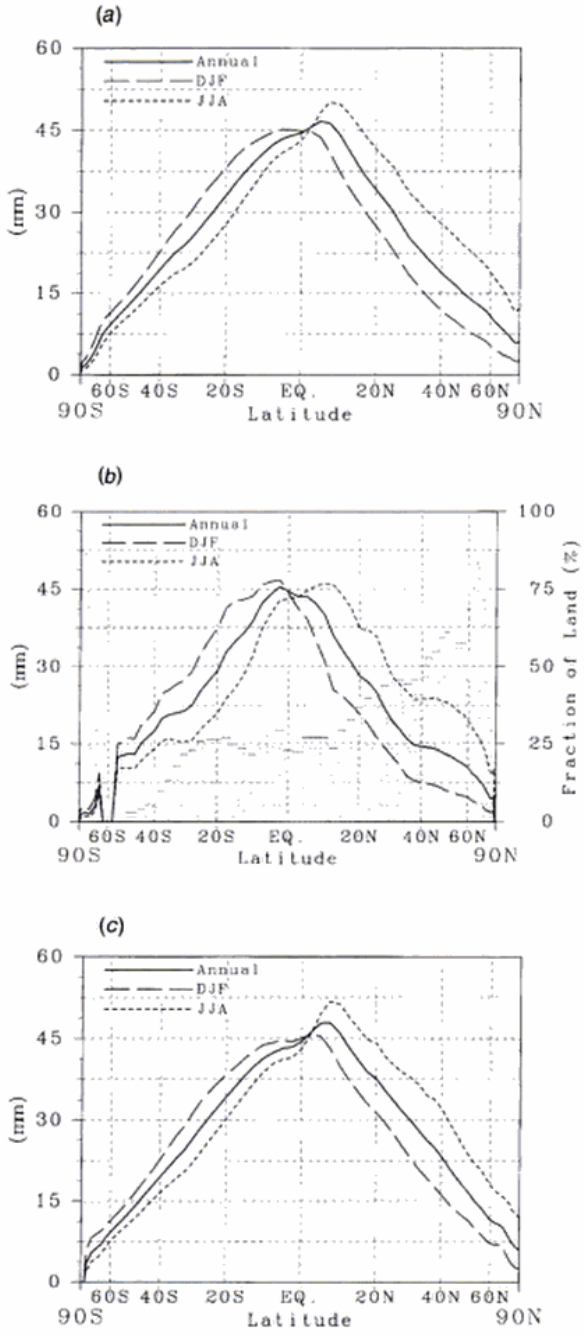

Figure 1.9. Meridional distribution of zonal mean precipitable water W, (*a*) over land and sea, (*b*) mean over land only, and (*c*) mean over sea only. Annual mean, December–January–February (DJF) mean, and June–July–August (JJA) mean for 4 years from 1989 to 1992.

regions are major convergence zones globally. In these areas, precipitation exceeds evapotranspiration. The deficit is made up of water coming from divergence zones, mainly over subtropical oceans. The north–south width of the tropical convergence zone is wider from the Indian Ocean to the western Pacific Ocean than elsewhere. The regions of high convergence generally correspond to the regions of high precipitable water. An exception is the convergence zone at the Pacific coast of North America near 50°N, where there are so-called storm tracks. While subtropical oceans are generally regions of divergence, parts of them include convergence zones, e.g., the South Pacific Convergence Zone (SPCZ) to the northeast of Australia in DJF and the Asian monsoon convergence zone in the western Pacific Ocean in JJA, which corresponds to the Bai-u Front.

The zonal mean $-\nabla_H \cdot \vec{Q}$ (Figure 1.11) shows relatively small seasonal changes at latitudes higher than 40°S and 40°N. Over land, in the regions within 20° of the Equator, the surface stores water from an excess of precipitation over evapotranspiration during the summer season and returns moisture to the atmosphere during the winter season. The situation is reversed between 40°N and 70°N. The values of $-\nabla_H \cdot \vec{Q}$ for DJF and JJA over land are fairly symmetric with positive (summer hemisphere) and negative (winter hemisphere) peaks at roughly 15°. However, over the sea, there are two negative peaks, at 20° for the winter hemisphere and at 25° for the summer hemisphere, but the positive peak of the Intertropical Convergence Zone (ITCZ) stays at 5°N to 10°N for the whole year. The peak is larger in JJA than DJF, which reflects the fact that the activity of the ITCZ is higher in the northern hemisphere's summer.

Global aspects of precipitation and evaporation

The global distributions of water fluxes at the surface are briefly introduced in this subsection. To illustrate the global distribution of precipitation, gridded global precipitation data by Xie and Arkin (1996) for the years 1989 to 1992 were employed. There are other published estimates, but all the long-term averages agree well over land. Large discrepancies exist over the oceans, but it is thought that estimates that include satellite information should be better. Xie and Arkin (1996) merged satellite data with rain-gauge observations and model estimates, and they also discussed the accuracy of their estimates. These are the reasons why their estimates are used here.

Zonal mean precipitation P is shown in Figure 1.12; overall, over land, and over sea. Annual precipitation overall and over sea have the largest peak at 10°N; however, the peak of annual precipitation over land stays at the equator. Zonal

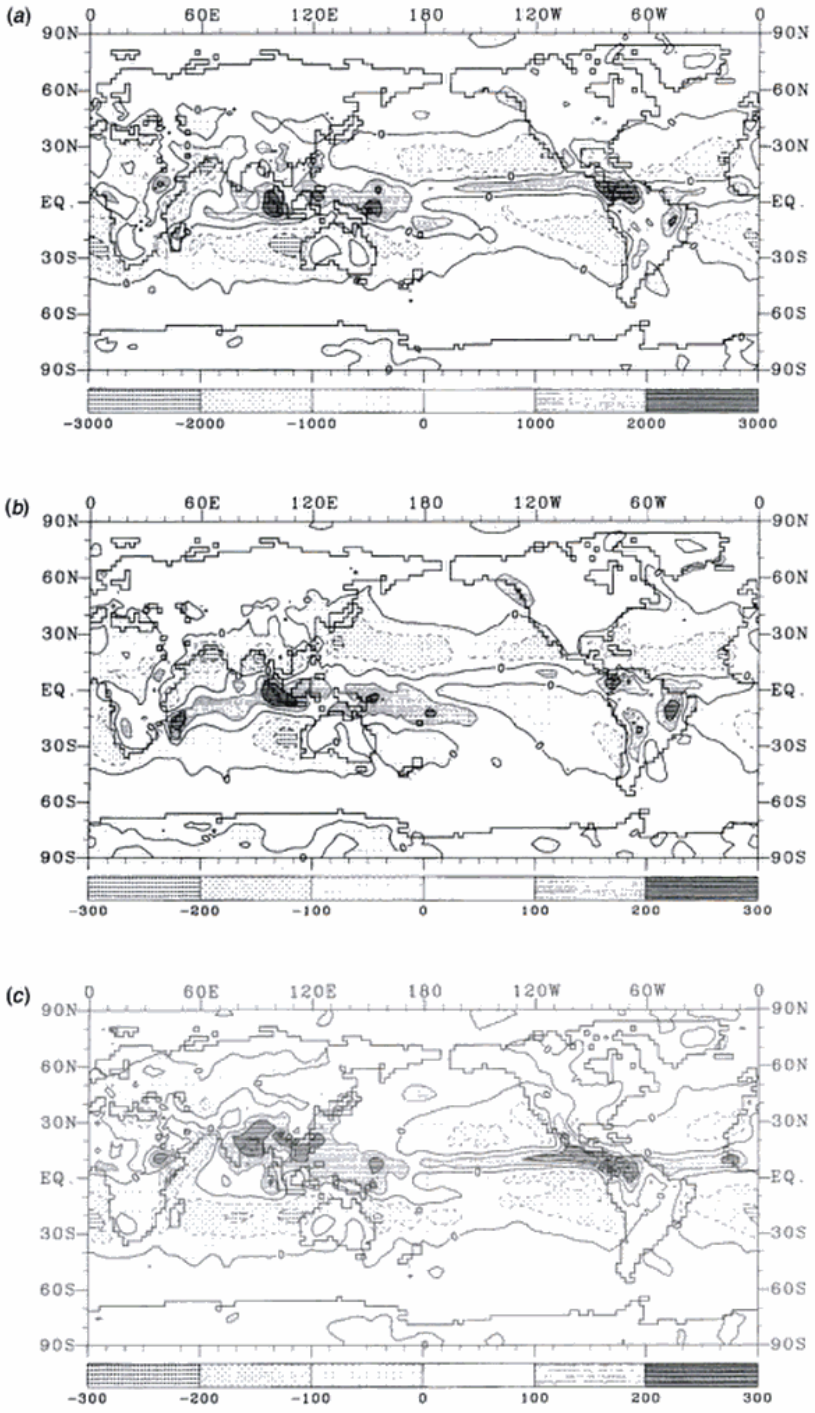

Figure 1.10. Global distribution of vertically integrated horizontal vapor flux convergence $-\nabla_H \cdot \vec{Q}$; (*a*) annual mean (mm yr^{-1}), (*b*) DJF mean (mm month^{-1}), and (*c*) JJA mean (mm month^{-1}). Four-year mean from 1989 to 1992 estimated from ECMWF 4 DDA.

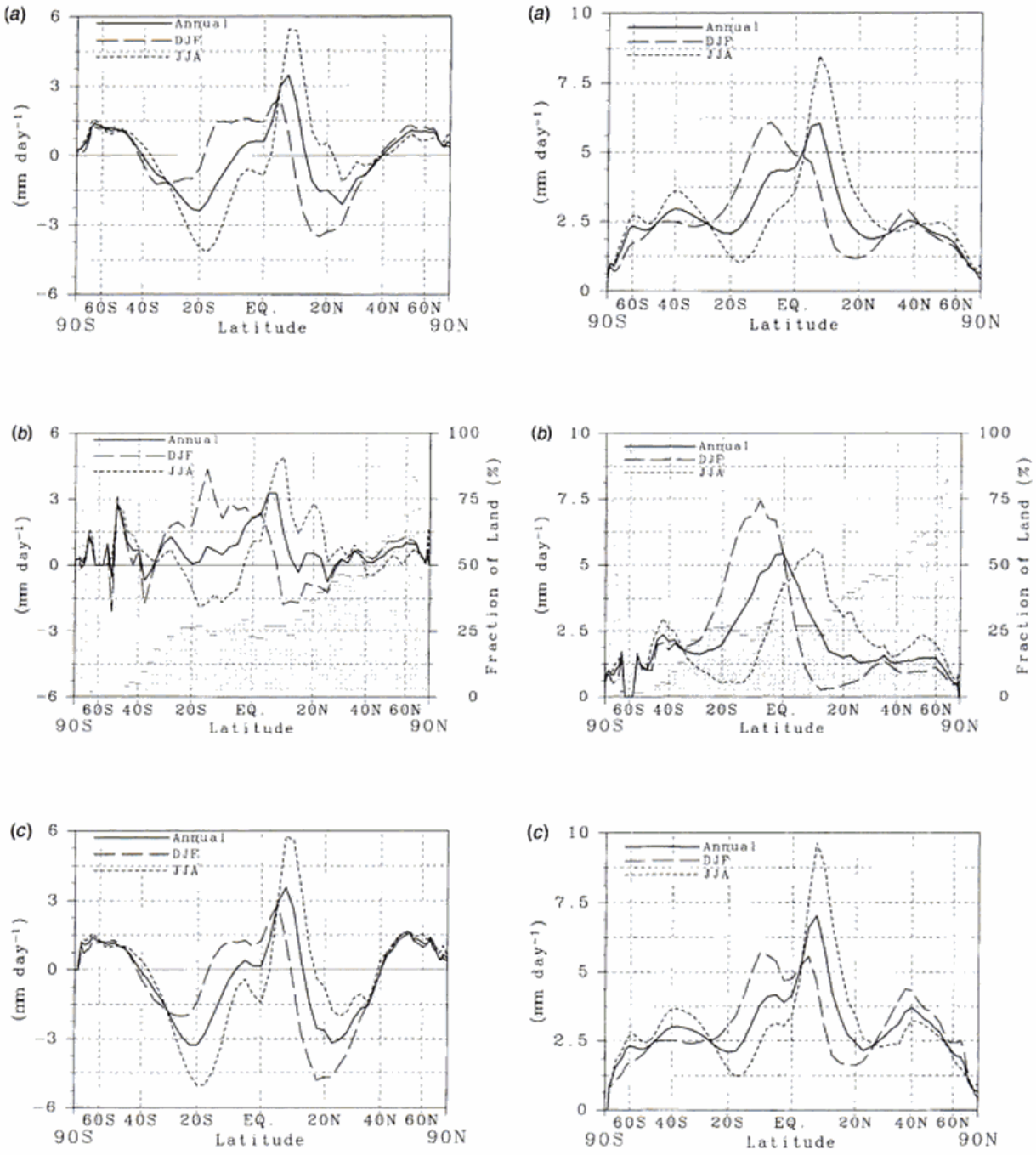

Figure 1.11. Meridional distribution of vertically integrated horizontal vapor flux convergence $-\nabla_H \cdot \vec{Q}$ for (*a*) over land and sea, (*b*) mean over land only, and (*c*) mean over sea only. Annual mean, DJF mean, and JJA mean for 4 years from 1989 to 1992.

Figure 1.12. Meridional distribution of zonal-mean precipitation by Xie and Arkin (1996) for (*a*) mean over land and sea, (*b*) mean over land only, and (*c*) mean over sea only.

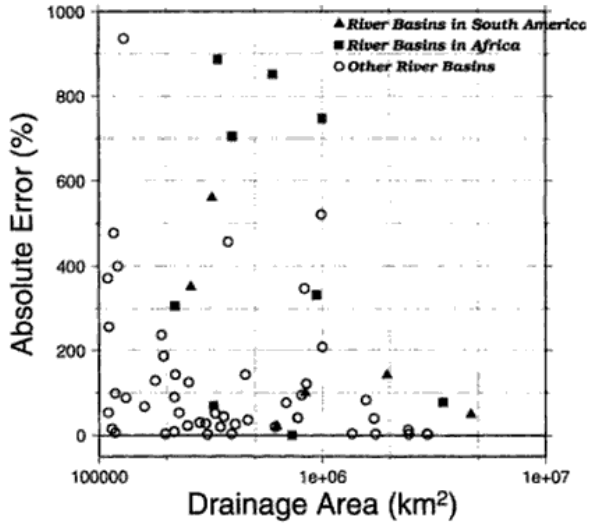

Figure 1.16. Absolute error (%) of annual water vapor flux convergence against climatological annual runoff. Dependency on the basin size is illustrated.

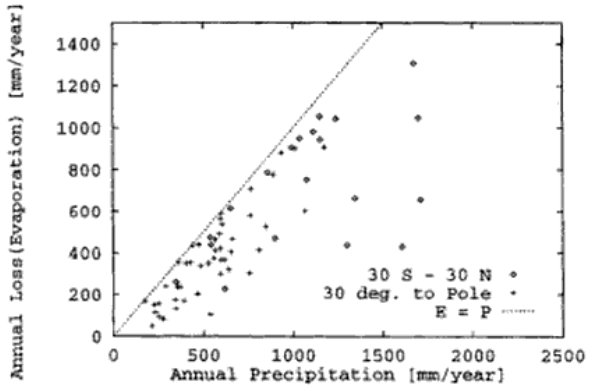

Figure 1.17. Mean water balance of major river basins. P is calculated from Xie and Arkin (1996), and E is calculated as $P - R$ using runoff R from GRDC data.

Phraya River basin in Thailand. Similar adjustments were applied for $-\nabla_H \cdot \vec{Q}$ of the 70 rivers (Oki *et al.*, 1995c). Consequently, from this atmosphere–river basin water balance method, the relative water storage as a function of time of year can be estimated, including the change of snow accumulation, soil moisture, groundwater table, and water storage in river channels.

The monthly water balance of climatological means in five individual river basins are shown in Figures 1.18 through 1.22. P is summarized from Xie and Arkin (1996), E by equation (1.2.11), $\vec{R}_o$ from the Global Runoff Data Centre (GRDC, 1992), and S by equation (1.2.12). The minimum value of S is set to zero. S represents the instantaneous value at the beginning of each month and other values are monthly totals. In the two tropical river basins, the Amazon (Figure 1.18) and the Zaire (Figure 1.19), monthly mean precipitation is above 50 mm month^{-1} throughout the year and the seasonal change of monthly runoff is small. In the case of the Mississippi river basin (Figure 1.20), the characteristics of monthly water balance are similar to that of the tropical rivers, but the excess of E over P from July to September is distinct. This characteristic has also been reported by Roads *et al.* (1994); however, the total water storage S (noted as W in Roads *et al.*, 1994) is somewhat different. The peak value for S of approximately 75 mm reported by Roads *et al.* (1994) occurred from March to April, while the peak of 100 mm occurs in June in Figure 1.20. The water balance of the Nile river basin is shown in Figure 1.21, which is relatively dry on average. The rainfall is 20–50 mm month^{-1} and the seasonal change of E, R, and S roughly follows the pattern of P. Finally, as a representative of a high-latitude river basin, the monthly water balance of the Ob river basin is shown in Figure 1.22. S increases until May and suddenly decreases with the increase of R. This corresponds to the snow accumulation and the melting runoff. An excess of E over P is estimated to occur during the warm season from May to July.

The accuracy of the estimates in Figures 1.18 to 1.22 should be questioned, especially the estimates of S, but it is a very difficult problem to compare the total water storage with actual observations on large scales. Field observations are point measurements and their representativeness is a critical issue. Satellite remote sensing can directly measure only shallow soil layers at the surface of nearly bare soil. Even though the realizations of soil moisture or water storage in general circulation models are varied and still uncertain, it may be worthwhile comparing the S obtained by the atmospheric water balance against a GCM result because it gives soil moisture and water storage on a large scale. A numerical experiment under climatological conditions, using the atmospheric general circulation model of the CCSR (Center for Climate System Research, University of Tokyo) and NIES (National Institute for Environmental Studies), produced very good results that correspond well with values of S estimated by the atmospheric water balance method (Oki *et al.*, 1995*a*). In the case of the Amazon river basin (Figure 1.23), the river water storage calculated in the associated river-routing model has a dominant role in the seasonal change of total water storage (Oki *et al.*, 1996).

The amplitude of the annual change of total water storage

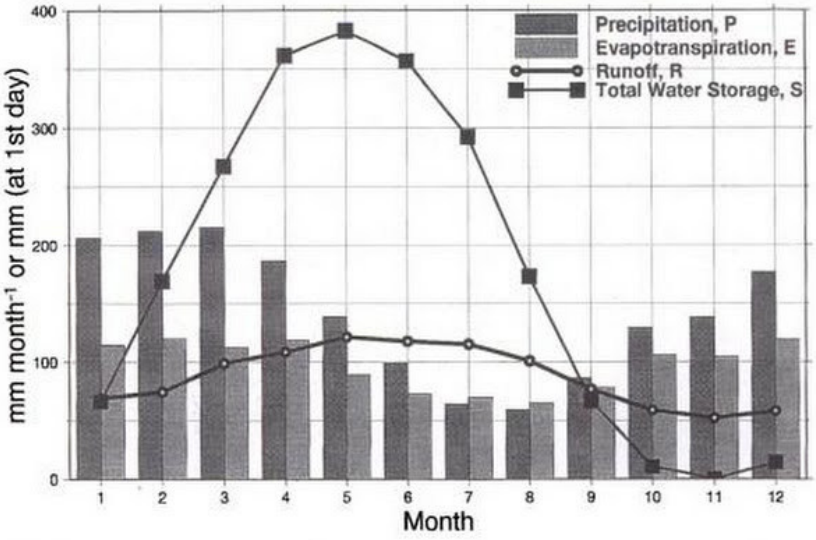

Figure 1.18. Water balance of the Amazon river basin. E and S are estimated using $-\nabla_H \cdot \vec{Q}$. P is estimated from Xie and Arkin (1996), and R from GRDC. Catchment areas are 6150 (total) and 4640 (at Obidos) $\times 10^3$ km^2.

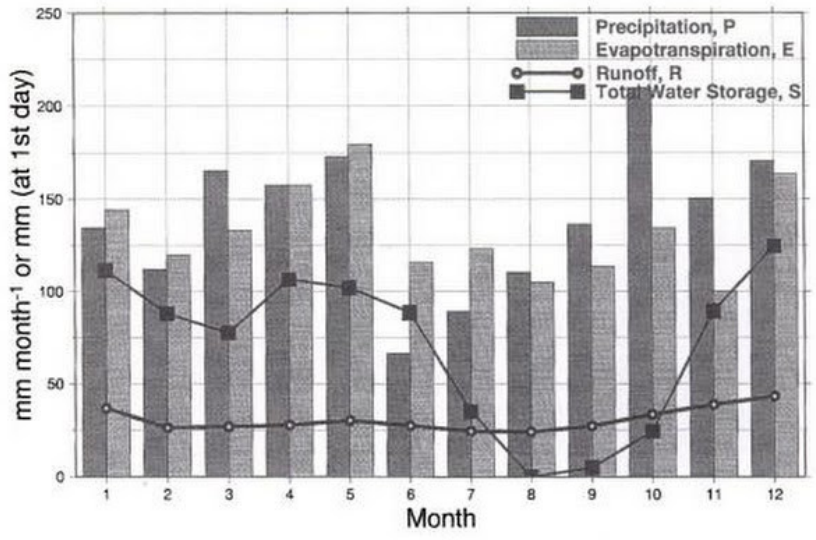

Figure 1.19. Water balance of the Zaire river basin. Catchment areas are 3690 (total) and 3475 (at Kinshasa) $\times 10^3$ km^2.

in each river basin for which data exist is mapped globally in Figure 1.24. It is large for the Amazon, Yenisey, Lena, and the rivers in Southeast Asia. Although these amplitudes include the change of snow accumulation and storage in river channels etc., roughly speaking, they should correspond to the amplitude of annual soil moisture change; the field capacity may be larger than this range. It is interesting and encouraging that only a few river basins have an annual change of total water storage larger than 200 mm, and the number of 200 mm is comparable to the values of field capacity of soil moisture in the land surface parameterizations of general circulation models.

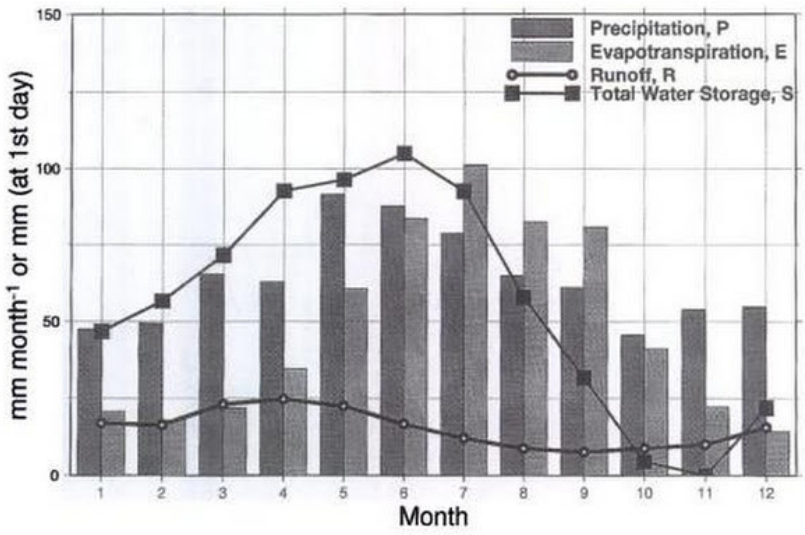

Figure 1.20. Water balance of the Mississippi river basin. Catchment areas are 3248 (total) and 2964 (at Vicksburg) $\times 10^3$ km^2.

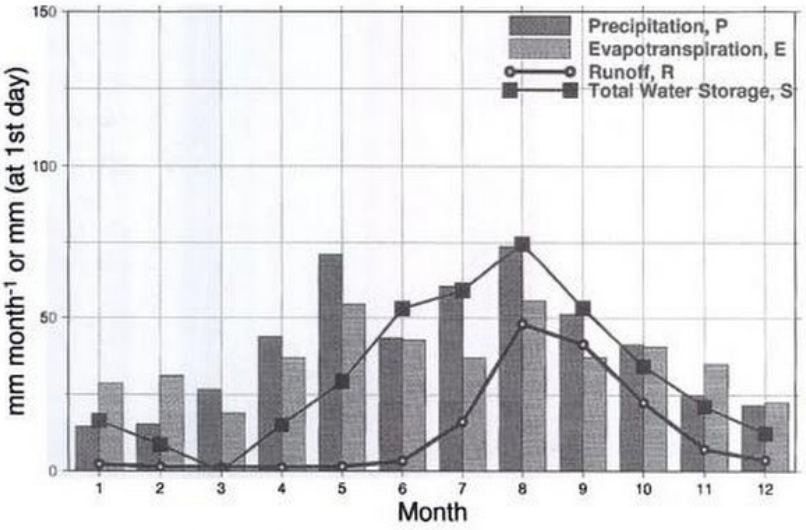

Figure 1.21. Water balance of the Nile river basin. Catchment areas are 3007 (total) and 325 (at Khartoum) $\times 10^3$ km^2.

Global aspects of freshwater distribution and fluxes into the ocean

The freshwater supply to the ocean has an important effect on the thermohaline circulation because it changes the salinity and thus the density. Annual freshwater transport by rivers and the atmosphere to each ocean is summarized in Table 1.4. Some part of the water vapor flux convergence remains in the inland basins. There are a few negative values in Table 1.4, suggesting that net freshwater transport occurs from the ocean to the continents. This is physically impossible and is caused by the errors in the source data. Although a detailed discussion of the values in Table 1.4 may not be meaningful, it is nevertheless interesting that such an analysis does make at

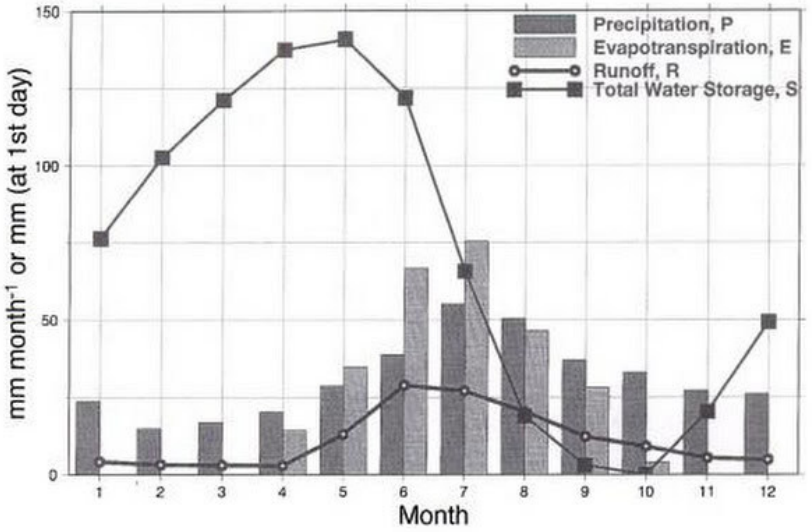

Figure 1.22. Water balance of the Ob river basin. Catchment areas are 2978 (total) and 2950 (at Salekhard) $\times 10^3$ km^2.

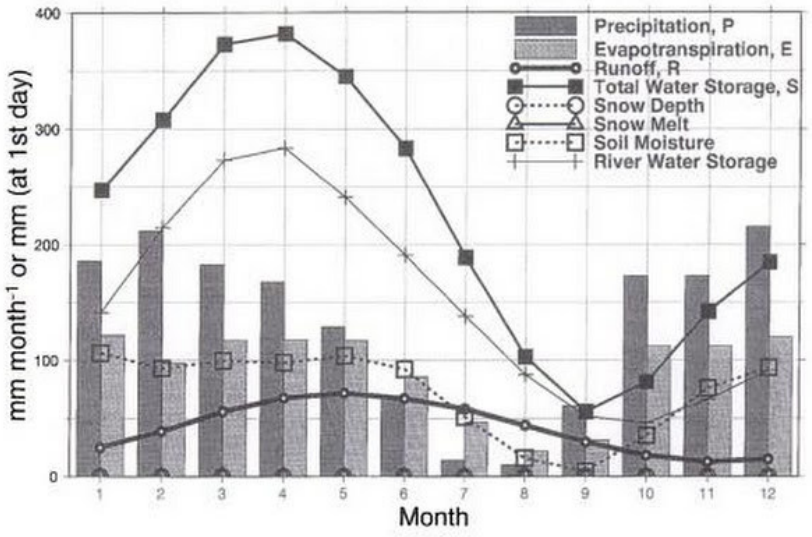

Figure 1.23. Water balance of the Amazon river basin calculated by an atmospheric GCM.

least qualitative sense using the atmospheric water balance method with geographical information on basin boundaries and the location of river mouths. In this analysis, it should be noted that the total amount of freshwater transport into the oceans from the surrounding continents has the same order of magnitude as the freshwater supply that comes directly from the atmosphere, expressed by $-\nabla_H \cdot \vec{Q}$.

The annual freshwater transport in the meridional direction has been estimated from equations (1.2.13) and (1.2.14) with results shown in Figure 1.25. The estimates in Figure 1.25 are the net transport; i.e., in the case of oceans, it is the residual of northward and southward freshwater flux by all ocean currents globally, and it cannot be compared directly with individual ocean currents such as the Kuroshio and the

Table 1.4. *Annual freshwater transport from continents to each ocean (10^{15} kg year^{-1}).*

		N.P.	S.P.	N.At.	S.At.	Indian	Arctic	Inner	Total
	Asia	4.7	0.4	0.2		3.3	2.7	0.1	11.4
	Europe			1.7		0.0	0.7		2.4
From	Africa			−0.2	0.9	−0.2		−0.4	0.1
rivers	N.America	2.9		4.8			1.1		8.8
	S.America	0.5	0.4	5.7	8.3				14.9
	Australia		0.1			0.1			0.2
	Antarctica		1.0		0.1	0.8			1.9
From	Total	8.1	1.9	12.2	9.3	4.0	4.5	−0.3	39.7
atmosphere	$-\nabla_H \cdot \vec{Q}$	9.9	−11.1	−12.7	−14.0	−14.0	2.2		−39.7
	Grand total	18.0	−9.2	−0.5	−4.7	−10.0	6.7	−0.3	0.0

Note: 'Inner' indicates the runoff to the inner basin within Asia and Africa.
$-\nabla_H \cdot \vec{Q}$ indicates the direct freshwater supply from the atmosphere to the ocean.
N.P., S.P., N.At., and S.At. represent North Pacific, South Pacific, North Atlantic, and South Atlantic Ocean.

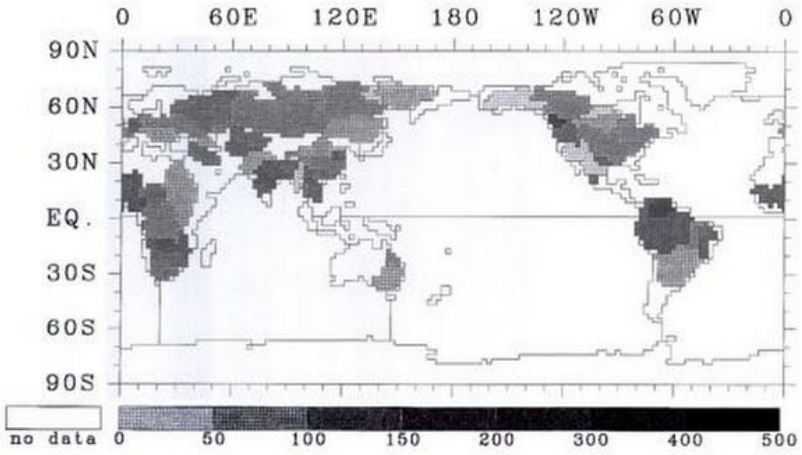

Figure 1.24. Amplitude of annual change of basin water storage (mm) estimated from ECMWF (1989–1992) and mean GRDC data.

Gulf Stream. Transport by the atmosphere and by the ocean have almost the same absolute values at each latitude but with different sign. The transport by rivers is about 10% of these other fluxes globally (this may be an underestimate because $-\nabla_H \cdot \vec{Q}$ tends to be smaller than river discharge observed at land surface). The negative (southward) peak by rivers at 30°S is mainly due to the Parana River in South America, and the peaks at the equator and 10°N are due to rivers in south America, such as the Magdalena and Orinoco. Large Russian rivers, such as the Ob, Yenisey, and Lena, carry the fresh water towards the north between 50–70°N.

These results indicate that the hydrologic processes over land play non-negligible roles in the climate system, not only by the exchange of energy and water at the land surface, but also through the transport of fresh water by rivers which affects the water balance of the oceans and forms a part of the hydrologic circulation on the Earth between the atmosphere, continents, and oceans.

Future prospects

The aim of Section 1.2 was not so much to show authoritative figures concerning the global aspects of the water cycle, but